https://doi.org/10.5194/acp-2021-99
Preprint. Discussion started: 18 March 2021

Atmospheric Chemistry and Physics Discussions

Aerosol formation and growth rates from chamber experiments using Kalman smoothing

Matthew Ozon[1], Dominik Stolzenburg[2], Lubna Dada[2], Aku Seppänen[1] and Kari E.J. Lehtinen[1,3]

[1] Department of Applied Physics, University of Eastern Finland, Kuopio, Finland
[2] Institute for Atmospheric and Earth System Research/ Physics, University of Helsinki, 00014 Helsinki, Finland
[3] Atmospheric Research Centre of Eastern Finland, Finnish Meteorological Institute, Kuopio, Finland

Correspondence to: Kari E.J. Lehtinen (kari.lehtinen@uef.fi)

Keywords. Particle number size distribution, nucleation, growth, chamber experiments, Bayesian state estimation, Kalman smoother, DMA train

Abstract.

Bayesian state estimation in the form of Kalman smoothing was applied to Differential Mobility Analyser Train (DMA-train) measurements of aerosol size distribution dynamics. Four experiments were analysed in order to estimate the aerosol size distribution, formation rate and size-dependent growth rate, as functions of time. The first analysed case was a synthetic one, generated by a detailed aerosol dynamics model, and the other three chamber experiments performed at the CERN CLOUD facility. The estimated formation and growth rates were compared with other methods used earlier for the CLOUD data and with the true values for the computer-generated synthetic experiment. The agreement in the growth rates was remarkably good for all studied cases. The formation rates matched also well, especially considering the fact that they were estimated from data given by two different instruments, the other being the Particle Size magnifier (PSM). The presented Fixed Interval Kalman Smoother (FIKS) method has clear advantages compared with earlier methods that have been applied to this kind of data. First, FIKS can reconstruct the size distribution between possible size gaps in the measurement in such a way that it is consistent with aerosol size distribution dynamics theory, and second, the method gives rise to direct and reliable estimation of size distribution and process rate uncertainties if the uncertainties in the kernel functions and numerical models are known.

1 Introduction

Atmospheric new particle formation and growth are important phenomena when considering global aerosol concentrations. Their concentration together with their size distribution and chemical composition determines how aerosols affect visibility, health and climate (Albrecht, 1989; Appel et al., 1985; Daellenbach et al., 2020; Pope and Dockery, 2006; Twomey, 1974). These are determined by atmospheric dynamics and aerosol dynamics such as new particle formation and growth as well as removal rates. Nieminen et al. (2018) reviewed the existing literature on the formation and growth rates ranging from polar sites, with very small aerosol concentrations to polluted urban sites with extremely high concentrations. The rates have been typically estimated using the methodology reviewed in Kulmala et al. (2012), based on rather simple regression or balance equation approaches, suffering from potentially crude approximations and permitting no proper estimation of the uncertainties. At the same time, however, instrument development, especially advances in particle detection efficiency and mass spectrometry, has developed rapidly

https://doi.org/10.5194/acp-2021-99
Preprint. Discussion started: 18 March 2021

Atmospheric Chemistry and Physics Discussions

(Kangasluoma et al., 2020). Potentially superior advanced data analysis methods have not been used, and, it is likely that there are significant inaccuracies in the estimated particle formation and growth rates estimated previously (Kürten et al., 2018).

There have been some attempts to estimate aerosol formation and growth rates with different inverse methods (Henze et al., 2004; Kuang et al., 2012; Lehtinen et al., 2004; Sandu et al., 2005; Verheggen and Mozurkewich, 2006; Viskari et al., 2012). We are, however, not aware of any of the above-mentioned methodology being used widely. The most promising ones in our view, that include also estimations of uncertainties, have been the ones by Kupiainen-Määttä (2016) and Shcherbacheva et al. (2020), who used Markov Chain Monte Carlo methodology to estimate evaporation rates as well as their uncertainties from synthetic cluster dynamics data. In addition, the INSIDE-method by Pichelstorfer et al. (2018), which is based on numerical solution of the aerosol general dynamic equation and matching the solution optimally to integrated measured concentrations of selected size intervals, has been successfully applied to determining growth rates at the CLOUD (Cosmics Leaving OUtdoor Droplets) experiments at CERN (European Organization for Nuclear Research) (Stolzenburg et al., 2020). Furthermore, the results in very recent manuscript by McGuffin et al. (2020), in which nucleation, growth and emission rates of are estimated using techniques from the field of nonlinear process control, seem promising.

In a recent paper, Ozon et al. (2020) presented BAYROSOL, a Julia software package that combines a finite difference solution to the general dynamic equation for aerosols (GDE; Seinfeld and Pandis, 2016) to Bayesian state estimation in order to estimate unknown size dependent process rates (nucleation, condensation, losses) from known time evolution of the aerosol size distribution. Using synthetic SMPS measurements Ozon et al., (2020) showed that the Fixed Interval Kalman Smoother (FIKS; Kaipio and Somersalo, 2005) performed very well in estimating the process rates of the GDE in two distinct cases. First in a case in which continuous nucleation, growth and losses lead to a nearly steady state size distribution and second also in a case in which there is a growing nucleation mode after a nucleation burst. In the method, the unknowns (such as the discretized particle size distribution) are modeled as random variables, and their prior probability distributions are incorporated in the solution of the inverse problem. One important key feature of the Kalman smoother method is that it estimates also the error covariance matrices of the process rates that is their uncertainties, if the uncertainties of the measurement device are known.

In this manuscript, we show results of applying BAYROSOL, for the first time to real experimental data. We use experiments performed with the differential mobility analyser-train (DMA-train; Stolzenburg et al., 2017) measuring new particle formation and growth at the CERN CLOUD chamber (Duplissy et al., 2016; Kirkby et al., 2011). In addition to testing the method with synthetic DMA-train data (in which the 'correct' results are known), we estimate formation and growth rates from three different formation and growth experiments: sulphuric-ammonia (Stolzenburg et al., 2020), alpha-pinene ozonolysis (Heinritzi et al., 2020) and iodic acid (He et al., 2021; Sipilä et al., 2016). We compare the formation rates with results obtained by using the methodology by Dada et al. (2020) based on Particle Size Magnifier (PSM) measurements and the growth rates with the results obtained by the INSIDE method (Pichelstorfer et al., 2018). We chose the DMA-train measurements for three main reasons: the high time resolution makes it an ideal instrument for nucleation studies, the collection efficiencies of the channels have been carefully characterized (Stolzenburg et al., 2017; Wlasits et al., 2020) and finally, the data from this instrument has not been used to estimate directly particle formation rates so far.

https://doi.org/10.5194/acp-2021-99
Preprint. Discussion started: 18 March 2021

Atmospheric Chemistry and Physics Discussions

2 Bayesian framework for parameter estimation

2.1 Aerosol measurement and evolution models

The quantities of interest in chamber experiments studying new particle formation are the particle number size-distribution, the formation rate at the critical cluster size and the growth rate of the freshly formed particles. The available measurements to infer these quantities usually size classify the aerosol and measure the size classified number concentrations. While the retrieval of the particle number size distribution from such measurements is a classical inverse problem (Chambolle and Pock, 2011; Kandlikar and Ramachandran, 1999; Wolfenbarger and Seinfeld, 1990), the estimation of the process parameters (formation and growth rate) is often done by analysis of the time evolution of the retrieved particle size distribution. Here, we focus on the formulation of the problem within a statistical Bayesian framework, where the state parameters described by a measurement model and an evolution model are treated as multivariate random processes and are estimated from measurements using a FIKS (Ozon et al., 2020).

A measurement can be described by a vector y^k representing m indirect observations (channels of the instrument) of the particle size distribution $n(d_p, t_k)$. The observations are linked to the size distribution by the so-called instrument transfer (or kernel) functions $\mathcal{H}$ such that:

$$y^k = \int \mathcal{H}(d_p) n(d_p, t_k) d d_p \quad (1)$$

The transfer functions $\mathcal{H}$ can be inferred from calibration experiments and instrument design considerations. Direct inversion of Eq. (1) for every time instant t_k is typically an underdetermined and ill-posed inverse problem and requires some additional assumptions in order to avoid oscillatory and unstable solutions (Kandlikar and Ramachandran, 1999). At the same time, the time evolution of the particle size-distribution $n(d_p, t)$ can be described by the aerosol general dynamic equation (GDE):

$$\frac{\partial n}{\partial t}(d_p, t) = -\frac{\partial g(d_p,t) n(d_p,t)}{\partial d_p} - \lambda(d_p, t) n(d_p, t) - \mathrm{CoagSink}(\beta, d_p, t) + \mathrm{CoagSrc}(\beta, d_p, t) \quad (2)$$

Here, $g(d_p, t)$ is the condensation growth/evaporation rate, $\lambda(d_p, t)$ is the particle loss by deposition or dilution and CoagSink and CoagSrc are the sink and source rates due to particle coagulation within the size distribution with the coagulation coefficients β. An exact expression of all terms can be found in e.g. Ozon et al. (2020) and Seinfeld and Pandis (2016). The boundary conditions of Eq. (2) are given by the apparent formation rate $J_{d_{min}}(t) = g(d_{min}, t) n(d_{min}, t)$ of newly formed particles at the minimum detectable size d_{min} and a zero numerical flux condition $g(d_\infty, t) n(d_\infty, t) = 0$ at very large sizes. Altogether, the process parameters $g(d_p, t), J(t), \lambda(d_p, t)$ and $\beta(d_i, d_j)$ as well as the initial and boundary conditions determine completely the evolution of the size distribution, but especially $g(d_p, t)$ and $J(t)$ are usually not known. The coagulation coefficients $\beta(d_i, d_j)$ can often be obtained from theory (and coagulation can be even neglected in many applications with low particle concentrations) and the loss parameters $\lambda(d_p, t)$ are well quantified for controlled aerosol chamber experiments.

A single measurement of the size distribution y^k does not depend explicitly on the process parameters, but as $g(d_p, t)$ and $J(t)$ determine the temporal evolution of $n(d_p, t_k)$ the estimation of the process parameters is feasible from a sequence of l measurements y^k at several time instances.

https://doi.org/10.5194/acp-2021-99
Preprint. Discussion started: 18 March 2021

Atmospheric Chemistry and Physics Discussions

2.2 State estimation with Kalman smoothing

Following Ozon et al. (2020) we formulate the problem as a Bayesian state estimation problem. After discretization of the problem in size space ($i = 1,..,q$) and time ($k = 1,...l$), we can define the state variable $X^k = [N_i^k \quad g_i^k \quad \lambda_i^k \quad J^k]$ for each time step k with the particle concentrations N_i^k per size discretization bin i, the condensation and loss terms g_i^k and λ_i^k , respectively, for each size discretization bin i and the nucleation rate J^k. The problem can then be formulated as:

$$X^{k+1} = F(X^k) + w^k \quad (3)$$

$$y^k = HX^k + v^k \quad (4)$$

Eq. (3) represents the discretized non-linear evolution model, which is based on the general dynamic equation for N^k, on second order processes for g^k and J^k, and a random walk evolution for λ^k (see Section 2.3). Eq. (4) represents the discretized linear observation model. The incorporation of positivity constraints for the process rates and the aforementioned second order models require minor modifications in the definition of the state variable X^k. This, however, does not cause any changes in the form of the state-space model (3)-(4). For the details on the above modifications as well as discretization of the GDE model, we refer to Ozon et al. (2020). The terms w^k and v^k are the error terms, which are approximated as normally distributed $\mathcal{N}(0, \Gamma_w^k)$ and $\mathcal{N}(0, \Gamma_e^k)$ with the covariance matrices Γ_w^k, Γ_v^k, which not only include stochastic noise, but also errors due discretization, model and parameter uncertainties. The GDE, i.e. the non-linear evolution model for N^k (Eq. (2)), is similar to an advection equation. Therefore, its numerical discretization schemes are often unstable and must be treated carefully to avoid oscillation and divergence or to minimize numerical diffusion (Shen et al., 2007; Smolarkiewicz, 1984). Thus, we show detailed considerations on the magnitude of the different error terms in the Supplement.

Algorithm 1 Extended Kalman Filter (EKF)

Initial state: Expectation $X^{0|0}$ and covariance $\Gamma^{0|0}$

for $k = 1,\ldots,l$

Prediction: expectation and covariance

$X^{k|k-1} = F(X^{k-1|k-1})$

$\Gamma^{k|k-1} = \partial F^{k-1}\Gamma^{k-1|k-1}(\partial F^{k-1})^T + \Gamma_w^{k-1}$

Kalman gain matrix:

$K^k = \Gamma^{k|k-1}(H^k)^T(H^k\Gamma^{k|k-1}(H^k)^T + \Gamma_v^k)^{-1}$

Measurement update: filter expectation and covariance

$X^{k|k} = X^{k|k-1} + K^k(Y^k - H^kX^{k|k-1})$

$\Gamma^{k|k} = (I - K^kH^k)\Gamma^{k|k-1}$

end

Algorithm 2 Fixed Interval Kalman Smoother (FIKS)

Initialization: Run Algorithm 1, store all variables

for $k = l-1,\ldots,1$

Backward gain matrix

$A^k = \Gamma^{k|k}(\partial F)^T(\Gamma^{k+1|k})^{-1}$

Smoother expectation and covariance

$X^{k|K} = X^{k|k} + A^k\left(X^{k+1|K} - X^{k+1|k}\right)$

$\Gamma^{k|K} = \Gamma^{k|k} + A^k(\Gamma^{k+1|K} - \Gamma^{k+1|k})(A^k)^T$

end

Table 1: Extended Kalman Filter and Fixed Interval Kalman Smoother algorithms for estimation of the state variables and their variances $\boldsymbol{X^k}$ and $\boldsymbol{\Gamma^k}$.

https://doi.org/10.5194/acp-2021-99
Preprint. Discussion started: 18 March 2021

Atmospheric Chemistry and Physics Discussions

Considering this structure of the problem, a non-linear extension to the Kalman Filter (Extended Kalman Filter; EKF) is a well suited algorithm for solving the unknown size-distribution and process parameters (Gelb, 1974; Kaipio and Somersalo, 2005). It is a two stage recursive procedure, where in the first stage the future state and propagation of error is predicted based on the state evolution model (Eq. (3)). In the second stage, the state variable and its covariance are estimated by updating the predicted state variable and covariance. This so-called measurement update accounts for the discrepancy between the realized measurements at time t_k and modelled measurements corresponding to the predicted state variable. This procedure is repeated until the final measurement $k = l$. After finishing the EKF recursions, we utilize a Fixed Interval Kalman Smoother (FIKS), which consists of a backward recursion from a backward gain matrix and smooths the results by backwards recursion from l to 1. The workflow of the EKF and FIKS are illustrated in Table 1 and more details on this algorithm can also be found in Ozon et al. (2020).

2.3 Adaption to chamber experiments

The state space model has been adjusted to represent best the evolution of an aerosol system during new particle formation experiments in an atmospheric simulation chamber like CLOUD. For the time evolution of the process parameters, we assume a rather smooth evolution for the nucleation and growth rates, approximated by a second order process (Ozon et al., 2020):

$$J^{k+1} = (r_1 + r_2)J^k - r_1 r_2 J^{k-1} + w_J^k \quad (5)$$

$$g^{k+1} = (r_1 + r_2)g^k - r_1 r_2 g^{k-1} + w_g^k \quad (6)$$

The constants r_1, r_2 depend on the characteristic time of change, discretization time and a dampening factor and their definition can be taken from (Ozon et al., 2020) and the corresponding values for our experiments are listed in Table S1 in the Supplement. The loss rates do not depend on time, in the chamber experiments of interest, and are well characterized by dedicated wall loss experiments (Stolzenburg et al., 2020). .The dilution time of the chamber $\tau_{dil} = Q_{tot}/V_{chamber}$. The time evolution is described by a random walk with a small stochastic noise term w_λ^k, and the expectation of the initial state is set to the experimentally determined value with a standard deviation of $\pm$10%:

$$\lambda^{k+1} = \lambda^k + w_\lambda^k \quad (7)$$

For fully defining the problem (Eq. (3)-(4)), an estimate of the covariance matrices corresponding to the error terms v^k and w^k is needed. The definition of the covariance matrices corresponding to the state noise w^k on the size-distribution evolution w_N^k, the growth rate w_g^k, the formation rate w_J^k and the wall loss rate w_λ^k follow the consideration of Ozon et al. (2020). The covariances of the wall losses, the growth rate and the size-distribution are dominantly diagonal with some additional off-diagonal terms in order to account for a correlation in size. The formulation given by Ozon et al. (2020) was slightly altered to give a stronger correlation between the closest size bins (values for the different experiments are given in Table S1 in the Supplement):

$$\Gamma_{N/g/\lambda}^k(i,j) = \sigma_{i,N/\lambda/g}\sigma_{j,N/\lambda/g} \exp\left(-\left(\frac{i-j}{\delta_{N/\lambda/g}}\right)^{a_{N/\lambda/g}}\right) \quad (8)$$

For the size-distribution evolution, we find that $\sigma_{i,\mathrm{N}}^2 = (\delta^k)^2 \mathrm{Var}(W_i^k)$, with δ^k the discretization time-step and W_i^k the error of the discretization of the size-distribution evolution. A detailed derivation of W_i^k is given in the Supplement.

The modelling error of the observation model and the measurement noise both contributing to v^k are assumed to be mutually independent. For this reason, the covariance of the error term Γ_v^k in the measurement model is written as a sum of the covariances of these two random variables, i.e. $\Gamma_v^k = \Gamma_{mod}^k + \Gamma_y^k$. For a detailed derivation we refer to the Supplement, where we also show that the discretization error is negligible compared to model and measurement error if

https://doi.org/10.5194/acp-2021-99
Preprint. Discussion started: 18 March 2021

Atmospheric Chemistry and Physics Discussions

a fine enough size discretization is chosen. We approximate Γ_v^k with uncorrelated processes, and hence the covariance matrices are of the diagonal form. For the measurement error, the variance is given by Poisson counting statistics in the case of a single-particle counting detector such as a condensational particle counter (CPC):

$$\Gamma_y^k(i,i) = y^k(i) \quad (9)$$

For the model uncertainty, we assume the variance of the kernel $\mathrm{Var}(\Delta H_{i,j})$ is composed of an uncertainty proportional to $H_{i,j}$ (for example due to an offset in the absolute calibration of the instrument) and a shifting size information error (for example discrepancy between set and actual classified size in a mobility spectrometer). It can then be formulated as (detailed values for the experiments under investigation can be found in Table S1 in the Supplement):

$$\Gamma_{mod}^k(i,i) = \sum_{j=1}^{q} \left(n(d_j)\Delta_j\right)^2 \mathrm{Var}(\Delta H_{i,j}) \quad (10)$$

3 Experimental methods

We use experimental data from the CERN CLOUD experiment (Duplissy et al., 2016; Kirkby et al., 2011) where we measured particle size-distributions in the sub-10 nm range with a DMA-train (Stolzenburg et al., 2017). The raw data obtained from the DMA-train is used as input for the analysis of three different sets of experiments performed in the atmospheric simulation chamber. The DMA-train instrument kernels are also used for modelling an instrument response to simulated size-distribution data in order to verify the general performance of the FIKS to DMA-train like data.

3.1 DMA-train

The DMA-train is an electrical mobility spectrometer, specifically designed to measure sub-10 nm size-distributions (Stolzenburg et al., 2017). Six identical DMAs are applied in parallel i.e. they sample through the same inlet. They are set to six distinct but fixed voltages and hence classified sizes. The charging state of the aerosol is pre-conditioned in two TSI Inc. Advanced Aerosol Neutralizers (Model 3088), each supplying three DMAs at 5.5 litre per minute (lpm) total flow. We use the Wiedensohler approximation (Wiedensohler, 1988) to describe the steady-state charge distribution at the DMA inlets. Kallinger and Szymanski (2015) showed that for the used neutralizers the steady-state charge distribution is still achieved for flow rates up to 5 lpm. After size classification, the aerosol is detected in condensation particle counters. Four channels are equipped with TSI Inc. Model 3776 ultrafine CPCs for detection of aerosols down to 2.5 nm. They were operated at reduced temperature settings in order to increase the detection efficiency of the smallest particles, achieving a 50% detection efficiency for particles as small as 2 nm (Wlasits et al., 2020). Two channels of the DMA-train were operated with particle counters specifically designed for sub-2 nm particle detection using diethylene glycol (DEG), an Airmodus Ltd. particle size magnifier (Model A10, PSM) and a TSI Inc. nano-Enhancer (Model 3777). Both are used as boosters to activate the particles, which are subsequently detected by either an Airmodus Ltd. CPC (Model A20, for the PSM) or a TSI Inc. CPC (Model 3772, for the nano-Enhancer). Both channels have a higher aerosol flow rate of 2.5 lpm resulting in a broader transfer function and higher transmission at the DMA compared to the 1.5 lpm sample flow in the other four channels. The sheath flow at the DMAs is kept constant at 15 lpm for all six channels.

The constant sampling at fixed sizes allows for either a higher time-resolution at large aerosol number concentrations or a higher sensitivity towards low number concentrations due to longer signal averaging times compared to a scanning or stepping differential mobility spectrometer. To increase the number of measured particle sizes, one DMA is still operated in an alternating mode, switching between 6.2 and 8 nm every ten seconds. The other DMAs are set to classify particles of 4.3, 3.2, 2.55, 2.2 and 1.8 nm. The instrument kernels are obtained from calibration experiments, where we use the

https://doi.org/10.5194/acp-2021-99
Preprint. Discussion started: 18 March 2021

Atmospheric Chemistry and Physics Discussions

DMA transfer function and sampling loss characterization from Stolzenburg et al. (2017), the CPC activation efficiencies from Wlasits et al. (2020) and the charging efficiency was tested to follow the Wiedensohler approximation in Tauber et al. (2020). The kernel functions for all seven classified sizes are shown in Fig. 1 for an instrument averaging time of 120 seconds, sulphuric acid-like test particles (using the Ammonium Sulfate detection efficiencies from Wlasits et al. (2020)) and including the detector flow rates of each condensation particle counter. Therefore, the kernels can be used to convert raw particle counts at the detecting CPCs into a particle size-distribution (within an inverse problem) and vice-versa. Note that for different chemical composition of the input particles, the CPC response might be different. Therefore, the kernels used for analysing experiments where particles were formed from oxidized organics (Kirkby et al., 2016) or from iodic acid (He et al., 2021) are different and approximated by the calibration curves for oxidized beta-caryophyllene and sodium chloride from Wlasits et al. (2020).

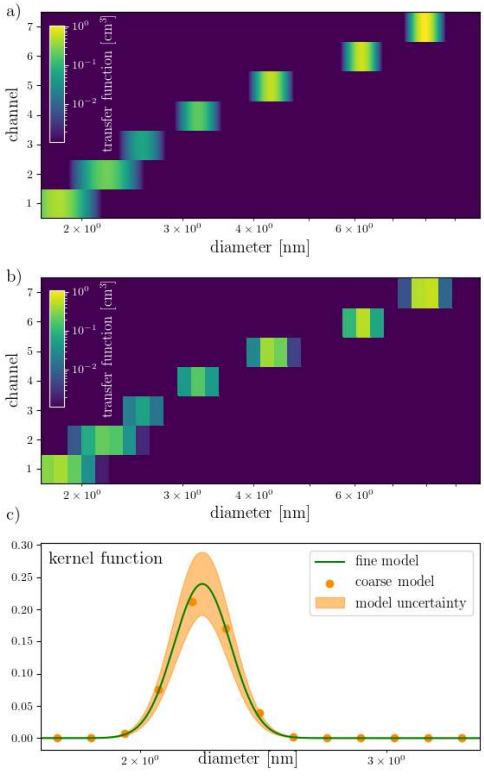

Figure 1: Kernel functions of the DMA-train when classifying sulphuric acid particles at a signal averaging time of 120 seconds. (a) shows the continuous form of the transfer function (color code) of the seven DMA-train channels (y-axis), inferred from instrument calibrations (Stolzenburg et al., 2017). (b) shows the discretization into 32 size bins from 1.7 to 10 nm used in the Kalman smoother (c) shows the comparison between continuous form and used discretization for channel 2 with centroid diameter at 2.2 nm, together with the model uncertainty, which is used for the error estimate (see Table S1 in the Supplement).

3.2 CLOUD

We use experimental data from the DMA-train measuring new particle formation in nucleation experiments at the CERN CLOUD chamber. The 26.1 m^3 stainless-steel chamber provides a high-purity, temperature-controlled environment in order to perform experiments under atmospherically relevant conditions, where trace gases can be added precisely at pptv (parts per trillion by volume) level and sunlight can be simulated by UV-illumination of the chamber. We use three

https://doi.org/10.5194/acp-2021-99
Preprint. Discussion started: 18 March 2021

Atmospheric Chemistry and Physics Discussions

different sets of experiments, of varying chemical composition, in order to demonstrate the performance of the FIKS in reconstructing formation and growth rates. See also Kirkby et al. (2011) and Duplissy et al. (2016).

First, a nucleation experiment using sulphuric acid and ammonia was performed at 5℃ by adding SO_2 and O_3 to the chamber and through the photo-dissociation of ozone, the formation of OH radicals and sulphuric acid was induced which resulted in strong new particle formation (Stolzenburg et al., 2020). Second, we performed nucleation and growth experiments at 5℃ using oxidized organics from dark (i.e. no UV-illumination) ozonolysis of alpha-pinene (Kirkby et al., 2016; Stolzenburg et al., 2018). Both experiments resulted in moderate new particle formation rate and thus, in the Kalman smoother, we used DMA-train data that was averaged over 120 seconds time intervals. Third, we studied nucleation from iodine oxides at 10℃ (He et al., 2021), which resulted in high particle formation rates and fast growth. For the third experiment, we reduced the DMA-train averaging time down to 20 seconds, while keeping high counting statistics over the averaging interval.

3.3 PSM derived formation rates

Particle formation rates (J_{dp}) are calculated from the time derivative of the total particle number concentration larger than 1.7 nm following the method introduced in Dada et al. (2020). The particle number size distribution is measured with the particle size magnifier (PSM) coupled with a condensation particle counter (1.5 – 2.5 nm), a TSI nano-SMPS (3 – 65 nm) and home-built long-SMPS (10 – 800 nm). The formation rates are corrected for the size dependent wall and coagulation losses. Additionally, since the chamber is operated in continuous mode, the particle concentrations are corrected for dilution losses. For more information on the PSM derived formation rates, see Dada et al. (2020). The uncertainty on $J_{1.7}$ was assumed to be 30% for the CLOUD chamber calculated using propagation of error in the concentration measurement, dilution, coagulation and wall losses as well as the error on the time-derivative of the total particle concentration.

3.4 Growth rates using INSIDE

In order to compare the particle growth rates derived by Kalman smoothing, we use the size- and time-dependent growth rate analysis tool INSIDE (Pichelstorfer et al., 2018). It uses input particle size-distributions at time t_1 in order to simulate the known aerosol dynamics (coagulation, wall losses and dilution) until a time t_2 (typically separated by one measurement cycle of an instrument, i.e. the 120 seconds averaging time mentioned above). At t_2, the simulated aerosol size-distribution is compared to the measured size-distribution and by evaluating the general dynamics equation above a certain diameter d_{eval} the growth term $\left.\frac{\mathrm{d}d_p}{\mathrm{d}t}\right|_{d_{\mathrm{eval}}} = \frac{\left.\frac{\mathrm{d}N_{\infty}}{\mathrm{d}t}\right|_{d_{\mathrm{eval}}}^{\infty} - \left.\frac{\mathrm{d}N_{\infty}^{sim}}{\mathrm{d}t}\right|_{d_{\mathrm{eval}}}^{\infty}}{\left.n(d_p,t)\right|_{d_{\mathrm{eval}}}}$ can be computed. Evaluating this equation for several evaluation diameters d_{eval} and at all measurement times t_i, this results in time- and size-resolved growth rates from a size-distribution measurement, which is distinct from most others, integrative growth rate analysis approaches (Dada et al., 2020). However, compared to the Kalman smoothing, each time step is analysed individually and the analysis framework relies on already inverted size distributions, where a point-by-point inversion procedure is used for the DMA-train data of this work (Stolzenburg and McMurry, 2008). Moreover, the INSIDE method does not provide an uncertainty estimate on the growth rate calculation and hence a comparison with other growth rate calculations is beneficial to verify the results.

https://doi.org/10.5194/acp-2021-99
Preprint. Discussion started: 18 March 2021

Atmospheric Chemistry and Physics Discussions

4 Results: Simulation and Experimental

4.1 Numerical simulation test

First, we modelled the DMA-train instrument numerically and simulated a data set representing a typical nucleation experiment performed in an atmospheric simulation chamber like CLOUD and applied the FIKS to this synthetic dataset. We used the same framework as in Ozon et al. (2020) to simulate a nucleation experiment with formation rate at 1 nm $J_{1.0} = 5.25\ \mathrm{cm}^{-3}\ \mathrm{s}^{-1}$, and size-independent growth rate $GR = 2.5\ \mathrm{nm\ h}^{-1}$ and the loss rates equal to the CERN CLOUD experiment (Stolzenburg et al., 2020). The evolution of the simulated size-distribution is shown in Fig. 2a. The measurement data y^k are then simulated using the kernel functions from Fig. 1a and altered with a Poisson-distributed random counting error. The FIKS is then applied to the measurement data with the input parameters given in Table S1 in the Supplement.

Figure 2 also shows the Kalman smoother estimates for the size-distribution, growth rate and formation rate at 1.7 nm. The reconstructed size-distribution (Fig. 2b) is very similar to the true size-distribution (Fig. 2a), especially taking into account the sparser discretization of the former. Also the estimated growth and nucleation rates agree well with true values of the respective process rates specified in the simulation. Moreover, the uncertainty estimates are feasible: For both quantities, the true values are within the uncertainty limits given by FIKS. The reconstructed size-distribution and especially, growth rate (Fig. 2 b and c, respectively) show some temporal oscillations, which are related to periods for the particle population to grow from the size range visible for one DMA-train channel to the next one. That is, the oscillation is a result of an insufficient coverage of the size-range by the DMA-train kernels and is discussed in more detail in Section 4.5. Nevertheless, the overall good retrieval of the simulated size distribution and process rates demonstrates that Kalman smoothing approach is well suited for analysing DMA-train data from chamber nucleation experiments.

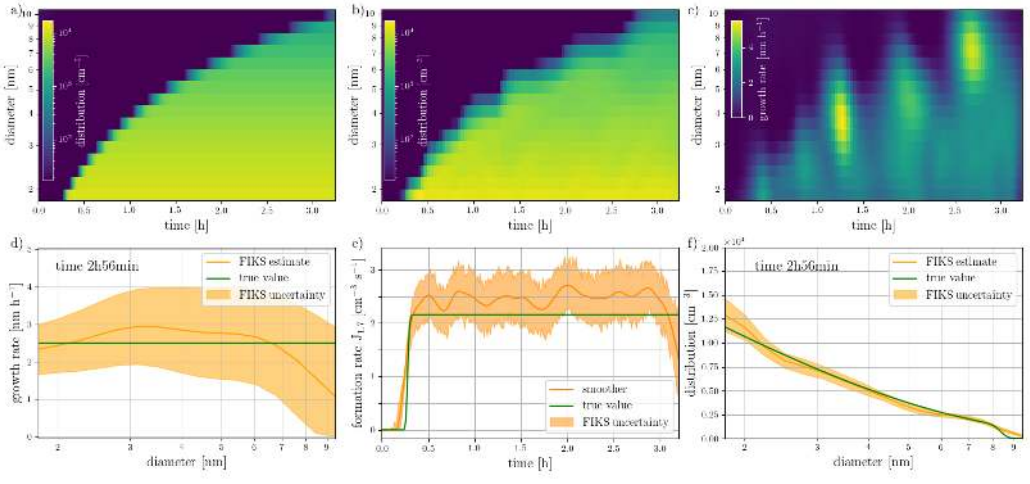

Figure 2: Results of the simulated chamber nucleation experiment: (a) The simulated, temporally evolving size distribution of aerosols. (b) The FIKS estimate for the size distribution. This estimate was computed based on the numerically simulated DMA-train data corresponding to the synthetic size distribution shown in (a). (c) The FIKS estimate for the growth rate of particles. (d) The growth rate corresponding to a single instant of time (2h 56min); here, the FIKS estimate and the associated uncertainty limits are plotted together with the true growth rate. (e) The FIKS estimate for the formation rate at 1.7 nm and its uncertainty, and the true formation rate. (f) FIKS estimate, its uncertainty and the true value of the particle size distribution corresponding to a single instant of time (2h 56min). In subfigures d-f, the orange lines represent the FIKS estimates (posterior expectations) and the orange shaded areas illustrate the uncertainties of the associated variables (more specifically, their approximate posterior standard deviation limits). The true values of the quantities are plotted in green.

https://doi.org/10.5194/acp-2021-99
Preprint. Discussion started: 18 March 2021

Atmospheric Chemistry and Physics Discussions

4.2 Sulphuric Acid-Ammonia experiment

We applied the FIKS to experimental data from a sulphuric acid-ammonia nucleation and growth experiment performed at 5℃ at the CERN CLOUD chamber. The raw data measured with the DMA-train were averaged in 120-second time intervals in order to increase the counting statistics per channel and then used as input for BAYROSOL. The details of parameter choices in FIKS are given again in Table S1 in the Supplement. The results of applying the Kalman smoothing to this experimental data are shown in Fig. 3.

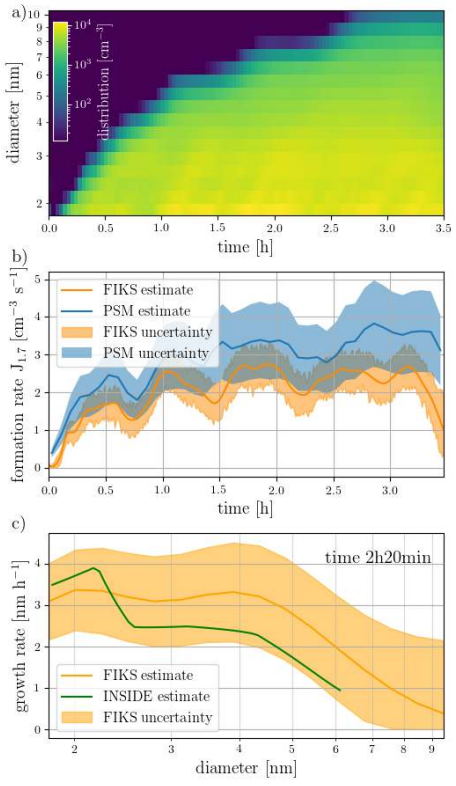

Figure 3: Results of an experiment performed at the CERN CLOUD chamber: The DMA-train data was acquired during sulphuric acid-ammonia nucleation and growth processes. Experimental conditions: 5°C, 60% RH, 5 ppb SO_2, 120 ppb O_3 and 40 ppt NH_3. (a) The FIKS estimate for the size distribution. (b) The evolution of the formation rate during the experiment. The orange line and shaded area represent the FIKS estimate and its uncertainty, respectively, while the solid blue line and blue area show the nucleation rate estimate and the associated 30% uncertainty based on a different set of instruments (particle size magnifier, PSM) and the standard approach for inferring nucleation rates at 1.7 nm (Dada et al., 2020). (c) The growth rate corresponding to time 2h19 min after the start of the experiment. The FIKS estimate and the associated uncertainty are marked with orange line and shaded area, respectively. The green line represents the growth rate estimate, which is obtained from DMA-train data by traditional inversion (INSIDE method).

The size- and time-dependence of the FIKS estimate for the true size-distribution (Fig. 3a) is very smooth, and it is also able to bridge the information gaps between the largest size-distribution channels. This is a significant improvement from the traditional point-by-point inversion, where the data of each DMA-train channel is inverted independently: When point-by-point inversion was applied to the same dataset, those information gaps caused severe reconstruction errors (discontinuities) in the size-distribution, see (Stolzenburg et al., 2020). The size-distribution shows also small temporal fluctuations. The fluctuations are even more clearly visible in the reconstructed evolution of the formation rate (Fig. 3b). Remarkably, the same fluctuations are also recovered when the formation rate is inferred from the PSM and nano-SMPS,

https://doi.org/10.5194/acp-2021-99
Preprint. Discussion started: 18 March 2021


Atmospheric Chemistry and Physics Discussions

i.e. an entirely different set of instrumentation and different type of data-analysis. This result strongly suggests that the fluctuation of the particle formation truly occurs physically in the experiment and is not a reconstruction error caused by instrument noise or a bias caused by the inversion method. The absolute values of the two independent formation rate estimates agree upon a factor of 1.5. Furthermore, large portions of the uncertainty intervals of these two estimates overlap with each other, which is another indicator of the feasibility of FIKS to analysing DMA-train data. In addition, also the inferred growth rates agree within the systematic uncertainties for both approaches (Fig. 3c for one time instant). It is worth noting, however, that both growth rate estimates rely on data from the same instrument and are hence more interdependent than the formation rate estimates. Nevertheless, the good agreement between them corroborates the feasibility of Kalman smoothing to reconstructing nanoparticle growth rates from experimental data.

4.3 Alpha-pinene ozonolysis experiment

Third, we applied the FIKS to experimental data obtained by the DMA-train from an alpha-pinene ozonolysis experiment. Besides the different chemical composition of the growing particles (resulting in different assumptions on the DMA-train transfer functions) in comparison to the experimental results used in section 4.2, this experiment is characterized by a different size-dependency of the growth rate, due to the increased condensation of low- and semi-volatile organics with increasing particle size (Simon et al., 2020; Stolzenburg et al., 2018; Tröstl et al., 2016). The formation rate, however, remains rather similar to the sulphuric acid-ammonia experiment under these specific experimental conditions, but the slower initial growth rates result in generally lower produced particle concentrations. The results of applying FIKS to the data from this experiment are shown in Fig. 4. Again, the size-distribution given by FIKS is much smoother than that obtained with a standard inversion procedure (see Heinritzi et al. (2020) for the same dataset inverted by the standard approach).

Because in alpha-pinene ozonolysis experiment the nucleation and growth rates were known to be similar to those in the sulphuric acid-ammonia experiment, the parameters of their evolution models were selected as in Section 4.2 (Table S1 in the Supplement). The formation rate is again slightly lower than the one obtained from the PSM. Considering the fact that inter-instrument deviations in sub-10 nm size-distribution measurements can be as large as one order of magnitude (Kangasluoma et al., 2020), the achieved agreement is remarkable, especially as some fluctuations within the chamber can again be reconstructed in both approaches. The retrieved growth rates from the FIKS estimate and the INSIDE method agree remarkably well and both show the increasing growth rates with increasing particle size up to 4.3 nm, an indication for a strong Kelvin-effect in organic condensation (Stolzenburg et al., 2018; Tröstl et al., 2016). The decreasing Kalman smoother estimate above 4.3 nm is related to the fact that the FIKS searches a smooth estimate of the growth rate (Eq. (6)), but at that point (2h30min after experiment start), practically no information from the size-distribution above 4.3 nm is available, resulting in a slow decrease towards zero. This is due to the strong smoothness a priori used in the FIKS algorithm (Table S1 in the Supplement). The INSIDE method does not report growth rates from regions with no information (Pichelstorfer et al., 2018) from the size-distribution and hence the estimate stops at 4.3 nm.

https://doi.org/10.5194/acp-2021-99
Preprint. Discussion started: 18 March 2021

Atmospheric Chemistry and Physics Discussions

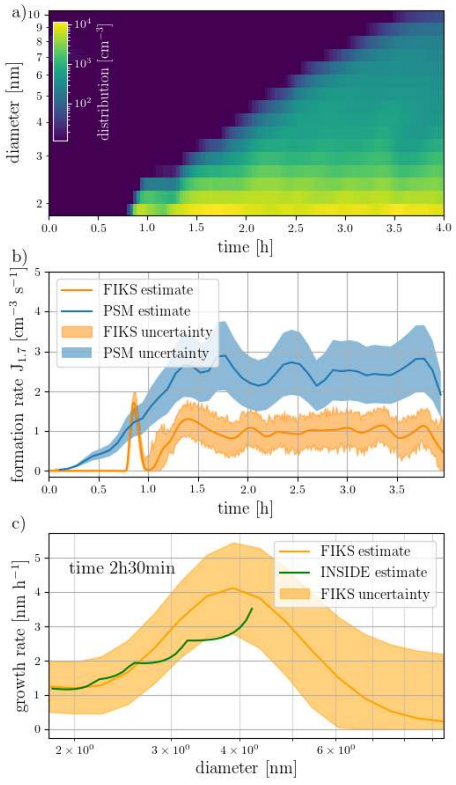

Figure 4: Results of an experiment performed at the CERN CLOUD chamber: The DMA-train data was acquired during an alpha-pinene ozonolysis. Experimental conditions: Experimental conditions: 5°C, 40% RH, 300 ppt alpha-pinene, 40 ppb O_3. (a) The FIKS estimate for the size distribution. (b) The evolution of the formation rate during the experiment. The orange line and shaded area represent the FIKS estimate and its uncertainty, respectively, while the solid blue line and blue area show the nucleation rate estimate and the associated 30% uncertainty based on a different set of instruments (particle size magnifier, PSM) and the standard approach for inferring nucleation rates at 1.7 nm (Dada et al., 2020). (c) The growth rate corresponding to time 2h30 min after the start of the experiment. The FIKS estimate and the associated uncertainty are marked with orange line and shaded area, respectively. The green line represents the growth rate estimate, which is obtained from DMA-train data by traditional inversion (INSIDE method).

4.4 Iodic Acid experiment

Finally, we analysed a more dynamic experiment of nucleation and growth from iodic acid (He et al., 2020, 2021). The experiment is characterized by extremely high nucleation rates, which are two orders of magnitude higher than in the sulphuric acid-ammonia and alpha-pinene ozonolysis experiments. However, the growth rate is only half an order of magnitude higher compared to the other two example cases. Figure 5 shows that, in spite of the highly dynamic experiment, the formation rate recovered by Kalman smoothing agrees with the estimate obtained from the PSM (Fig. 5b). The usage of the DMA-train data with a time resolution of 20 seconds allows for the precise recovery of the spike in formation rate in the beginning of the experiment. This causes the build-up of a high condensation sink and vapour/cluster depletion almost shutting off any further nucleation during the continuation of the experiment. The four-minute time resolution of the data for the calculation of the nucleation rate from the PSM is limited in that respect. The reconstructed growth rates (Fig. 5c) show again agreement between the FIKS estimate and the INSIDE method, indicating a clear decreasing trend with size, which is expected for condensation at the kinetic limit if the vapour molecular size is taken into account (He et al., 2021; Lehtinen and Kulmala, 2003; Nieminen et al., 2010; Stolzenburg et al., 2020). The lower

https://doi.org/10.5194/acp-2021-99
Preprint. Discussion started: 18 March 2021

Atmospheric Chemistry and Physics Discussions

values towards 1.8 nm could be caused by a biased estimate of the PSM detection efficiency, because neither a calibration for iodic acid clusters nor for sodium chloride particles (which was used for the other detectors in the DMA-train) was available. The instabilities in the size-distribution at the smallest sizes and fluctuations of the formation rate are expected considering the highly dynamic process of this experiment Overall, the good agreement for the inferred process parameters of the aerosol general dynamics equation, i.e. the formation and growth rates, is still remarkable. However, the reconstructed size-distribution from the FIKS estimate shows some discontinuities, especially during the growth above 3 nm. This is because the available instrument information from the DMA-train starts to get very sparse in that size range given the dynamic processes involved in the iodic acid nucleation and growth. More available size channels (hence more DMAs in the case of the DMA-train) would help to resolve such discontinuities. We will therefore provide an instrument design recommendation based on simulated data in the next section.

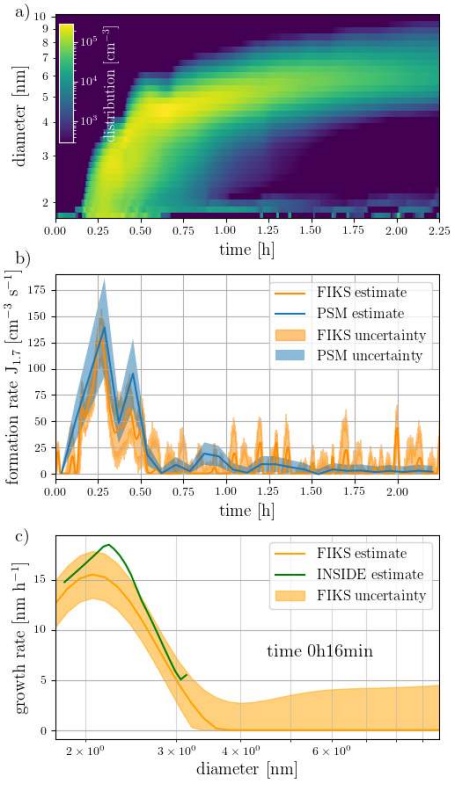

Figure 5: Results of an experiment performed at the CERN CLOUD chamber: The DMA-train data was acquired during iodic acid nucleation and growth processes. Experimental conditions: Experimental conditions: 10°C, 80% RH, 100 ppt I_2, 40 ppb O_3. (a) The FIKS estimate for the size distribution. (b) The evolution of the formation rate during the experiment. The orange line and shaded area represent the FIKS estimate and its uncertainty, respectively, while the solid blue line and blue area show the nucleation rate estimate and the associated 30% uncertainty based on a different set of instruments (particle size magnifier, PSM) and the standard approach for inferring nucleation rates at 1.7 nm (Dada et al., 2020). (c) The growth rate corresponding to time 0h16min min after the start of the experiment. The FIKS estimate and the associated uncertainty are marked with orange line and shaded area, respectively. The green line represents the growth rate estimate, which is obtained from DMA-train data by traditional inversion (INSIDE method).

4.5 Instrument design recommendation from a signal processing point of view

The size range covered by the seven DMA-train channels was chosen semi-arbitrarily based on some external constraints: the lowest measured centroid diameter was supposed to be as close as possible to 1.7 nm where the formation rate is

https://doi.org/10.5194/acp-2021-99
Preprint. Discussion started: 18 March 2021

Atmospheric Chemistry and Physics Discussions

typically measured for experiments performed at the CLOUD chamber. In order to cover the sub-10 nm range the largest channels was set to 8 nm. The other channel diameters were chosen to yield sufficient coverage of the sub-3 nm range. The width of the transfer functions was fixed by the detector sample flow rates and the 15 lpm critical orifices provided by Grimm Aerosol for the DMA sheath air supply (also the standard flow rate used by the manufacturer for this type of DMA). However, the chosen centroid diameters (and hence fixed voltages at the DMAs) and selected sheath flow rates could easily be altered.

In order to study numerically the effect of choice for the DMA-train channels, we constructed a model corresponding to a channel choice different from that in the previous sections: The kernel for the DMA-train with seven channels having centroid diameters of 1.8, 2.2, 2.8, 3.6, 4.6, 6.1 and 8.0 nm is illustrated in Fig. 6a. Moreover, channels 3 to 7 have been altered to use a 2.5 lpm sample flow rate (could be achieved by a make-up flow at each CPC) and a reduced sheath flow rate of 10 lpm, only providing a resolution of theoretical non-diffusive resolution of ~4, which is significantly lower. However, this permits covering the entire size-range between 1.8 and 8 nm by overlapping channels. We revisited the numerical simulation described in Section 4.1 using DMA-train model corresponding to this configuration. The resulting size-distribution given by FIKS is shown in Fig. 6b. Comparison between the two reconstructions in Fig. 2b and Fig. 6b reveals that the new choice of DMA-channels stabilizes the size-distribution estimate significantly. While in Fig. 2b, the size distribution evolves in step-wise manner when the growing particle mode reaches larger size-channels, the size distribution in Fig. 6b is very smooth, also temporally. The latter estimate also resembles the true (simulated) size-distribution (Fig. 2a) more than the former one.

The result of this additional numerical study thus demonstrates that in the chosen conditions of the simulation, the reconstruction quality improves when the resolution of individual channels is lowered. This seemingly counterintuitive effect stems from the fact that FIKS estimates do not rely only on the measurements, but are also advised by the GDE model, which makes the problem of optimizing the measurement design a somewhat cumbersome task. A rigorous investigation of the optimal experimental design is out of the scope of this paper, but the above observation is worth noticing -- especially because a lot of recent experimental effort in the sub-10 nm range has been devoted to improving the instrument resolution (Kangasluoma et al., 2020). While on the individual channel level this might reduce systematic uncertainties, as discussed in Kangasluoma et al. (2020), signal processing rather requires a broad coverage of the size distribution than high resolution. However, the ideal instrument would combine both, full coverage of the size distribution but achieved with more, high-resolution channels. For the DMA-train principle, this would require new ideas in instrument design in order to incorporate more DMAs without the instrument becoming impractically bulky.

https://doi.org/10.5194/acp-2021-99
Preprint. Discussion started: 18 March 2021

Atmospheric Chemistry and Physics Discussions

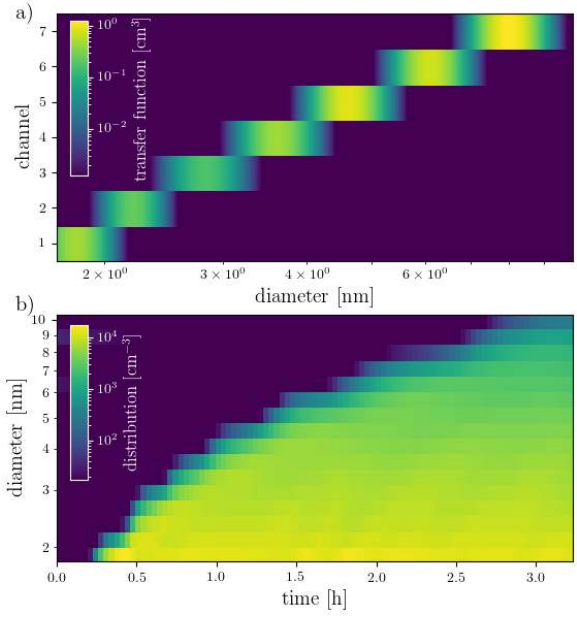

Figure 6: Adjusted DMA-train kernel for better signal processing (a), which could be achieved by choosing suitable centroid voltages and altering the resolution of the DMAs through sheath-flow and sample-flow adjustments. (b) shows the reconstructed simulated size-distribution of Fig. 2 using the adjusted kernel.

5 Conclusion

A recently developed methodology (BAYROSOL) applying the Fixed Interval Kalman Smoother (FIKS) to a finite difference solution to the aerosol GDE was used to analyze DMA-train measurements of aerosol dynamics at the CLOUD chamber facility at CERN. The overall aim of this methodology is to estimate unknown aerosol microphysical process rates as well as their uncertainties from size-distribution evolution measurements. In a previous paper, the methodology was shown to be able to predict new particle formation, growth and loss rates from synthetic computer-generated aerosol size distribution evolution data, while here the method has been applied to real experimental data for the first time. Four experimental cases with particle formation and growth were tested: 1) a computer-generated synthetic case, 2) sulphuric acid-ammonia, 3) alpha-pinene ozonolysis, and 4) iodic acid.

The DMA-train was selected for two main reasons: first, the instrument kernel functions are well characterized giving rise to reliable estimation of the instrument uncertainties and second, new particle formation rates have not been estimated directly from DMA-train measurements before. In addition, as the current version of the DMA-train is designed in such a way that the individual DMAs have a rather narrow collection kernels for the channels, with significant gaps between some of the channels, the FIKS can reconstruct the size distributions from the measured signals in such a way that the distributions are rather smooth and consistent with the GDE.

We compared the growth rates, which with BAYROSOL can be estimated as functions of both size and time, with those obtained by INSIDE, a method applied earlier to CLOUD data, and the agreement was remarkably good for all studied cases. INSIDE is also based on matching the GDE solution to measured size distribution dynamics, however without the capability of estimating uncertainties of the estimations. The FIKS-based estimates for the particle formation rates were compared with those estimated from data obtained by a separate instrument, the Particle Size Magnifier (PSM), based on

https://doi.org/10.5194/acp-2021-99
Preprint. Discussion started: 18 March 2021


Atmospheric Chemistry and Physics Discussions

the rate of change of the total number concentration measured by the instrument corrected by coagulation and wall-losses. Again, the agreement was very good, especially considering the fact that instrument uncertainties are large at the very lowest end of the measured size spectrum. For the iodic-acid case, the FIKS estimate of the formation rate was even able to capture rapidly changing dynamics of the experiment. It was remarkable for all cases that some fluctuations in the formation rates were recovered by both methods independently, indicating that these are physical variations during the experiment

Finally, we utilized the FIKS from an instrument development point of view. Typically, an as-high-as-possible resolution for the different measurement channels has been the aim when measuring nanometer-sized particles. This aim, however, gives rise to gaps in the measured size range, as is the case in the DMA-train studied. Thus we studied whether a better coverage of the size spectrum, but lower resolution of the individual channels would be advantageous for size distribution estimation.

Summarizing, we believe that Bayesian state estimation methods such as FIKS can be very useful in the field of aerosol science in many aspects. As mentioned above, they can be used to fill gaps in measurements in such a way that not only the obtained size distributions but also unknown process rates are consistent with theory describing aerosol size distribution dynamics. In addition, the methodology provides estimations of uncertainties both for size distributions as well as process rates based on uncertainty estimations in the measurements and the used models, which is unfortunately not common when reporting results of aerosol measurements. Finally, it is conceivable that the methodology presented here will be superior to several previous approaches when combining measurement data obtained with several different instruments that operate at different size ranges. This will be a topic of our forthcoming studies.

Data availability

The version of the implementation of the estimation method (BAYROSOL1.1)[https://doi.org/10.5281/zenodo.4450492] is available under the MIT Expat License; it is the version used to generate the results discussed in this paper. The package also contains the code used to obtain the results discussed in Ozon et al. 2020. It is possible to generate the simulated data described in section 4.1. The experimental data (DMA-train kernels) and raw data, are also included in the repository.

Competing interest

The authors declare no competing interests.

Acknowledgements

This publication has been produced within the framework of the EMME-CARE project, which has received funding from the European Union's Horizon 2020 Research and Innovation Programme (under grant agreement no. 856612) and the Government of Cyprus. This research has also received funding from the European Union's Horizon 2020 research and innovation programme under the Marie Sklodowska-Curie grant agreement no. 895875 ("NPF-PANDA") as well as Academy of Finland Project #325647. The sole responsibility of this publication lies with the author. The European Union is not responsible for any use that may be made of the information contained therein.

https://doi.org/10.5194/acp-2021-99
Preprint. Discussion started: 18 March 2021

Atmospheric Chemistry and Physics Discussions

Author contributions

MO, DS, LD analysed the experimental data, MO developed the software, all authors were involved in the scientific discussion and in the writing of the manuscript.

References

Albrecht, B. A.: Aerosols, Cloud Microphysics, and Fractional Cloudiness, Science, 245(4923), 1227–1230, doi:10.1126/science.245.4923.1227, 1989.

Appel, B. R., Tokiwa, Y., Hsu, J., Kothny, E. L. and Hahn, E.: Visibility as related to atmospheric aerosol constituents, Atmos. Environ., 19(9), 1525–1534, doi:https://doi.org/10.1016/0004-6981(85)90290-2, 1985.

Chambolle, A. and Pock, T.: A First-Order Primal-Dual Algorithm for Convex Problems with Applications to Imaging, J. Math. Imaging Vis., 40(1), 120–145, doi:10.1007/s10851-010-0251-1, 2011.

Dada, L., Lehtipalo, K., Kontkanen, J., Nieminen, T., Baalbaki, R., Ahonen, L., Duplissy, J., Yan, C., Chu, B., Petäjä, T., Lehtinen, K., Kerminen, V.-M., Kulmala, M. and Kangasluoma, J.: Formation and growth of sub-3-nm aerosol particles in experimental chambers, Nat. Protoc., doi:10.1038/s41596-019-0274-z, 2020.

Daellenbach, K. R., Uzu, G., Jiang, J., Cassagnes, L.-E., Leni, Z., Vlachou, A., Stefenelli, G., Canonaco, F., Weber, S., Segers, A., Kuenen, J. J. P., Schaap, M., Favez, O., Albinet, A., Aksoyoglu, S., Dommen, J., Baltensperger, U., Geiser, M., El Haddad, I., Jaffrezo, J.-L. and Prévôt, A. S. H.: Sources of particulate-matter air pollution and its oxidative potential in Europe, Nature, 587(7834), 414–419, doi:10.1038/s41586-020-2902-8, 2020.

Duplissy, J., Merikanto, J., Franchin, A., Tsagkogeorgas, G., Kangasluoma, J., Wimmer, D., Vuollekoski, H., Schobesberger, S., Lehtipalo, K., Flagan, R. C., Brus, D., Donahue, N. M., Vehkamäki, H., Almeida, J., Amorim, A., Barmet, P., Bianchi, F., Breitenlechner, M., Dunne, E. M., Guida, R., Henschel, H., Junninen, H., Kirkby, J., Kürten, A., Kupc, A., Määttänen, A., Makhmutov, V., Mathot, S., Nieminen, T., Onnela, A., Praplan, A. P., Riccobono, F., Rondo, L., Steiner, G., Tome, A., Walther, H., Baltensperger, U., Carslaw, K. S., Dommen, J., Hansel, A., Petäjä, T., Sipilä, M., Stratmann, F., Vrtala, A., Wagner, P. E., Worsnop, D. R., Curtius, J. and Kulmala, M.: Effect of ions on sulfuric acid-water binary particle formation: 2. Experimental data and comparison with QC-normalized classical nucleation theory, J. Geophys. Res.-Atmos., 121(4), 1752–1775, doi:10.1002/2015JD023539, 2016.

Gelb, A.: Applied optimal estimation, MIT Press, Cambridge, Massachusetts., 1974.

He, X.-C., Iyer, S., Sipilä, M., Ylisirniö, A., Peltola, M., Kontkanen, J., Baalbaki, R., Simon, M., Kürten, A., Tham, Y. J., Pesonen, J., Ahonen, L. R., Amanatidis, S., Amorim, A., Baccarini, A., Beck, L., Bianchi, F., Brilke, S., Chen, D., Chiu, R., Curtius, J., Dada, L., Dias, A., Dommen, J., Donahue, N. M., Duplissy, J., El Haddad, I., Finkenzeller, H., Fischer, L., Heinritzi, M., Hofbauer, V., Kangasluoma, J., Kim, C., Koenig, T. K., Kubečka, J., Kvashnin, A., Lamkaddam, H., Lee, C. P., Leiminger, M., Li, Z., Makhmutov, V., Xiao, M., Marten, R., Nie, W., Onnela, A., Partoll, E., Petäjä, T., Salo, V.-T., Schuchmann, S., Steiner, G., Stolzenburg, D., Stozhkov, Y., Tauber, C., Tomé, A., Väisänen, O., Vazquez-Pufleau, M., Volkamer, R., Wagner, A. C., Wang, M., Wang, Y., Wimmer, D., Winkler, P. M., Worsnop, D. R., Wu, Y., Yan, C., Ye, Q., Lehtinen, K., Nieminen, T., Manninen, H. E., Rissanen, M., Schobesberger, S., Lehtipalo, K., Baltensperger, U., Hansel, A., Kerminen, V.-M., Flagan, R. C., Kirkby, J., Kurtén, T. and Kulmala, M.: Determination of the collision rate coefficient between charged iodic acid clusters and iodic acid using the appearance time method, Aerosol Sci. Tech., 1–12, doi:10.1080/02786826.2020.1839013, 2020.

He, X.-C., Tham, Y. J., Dada, L., Wang, M., Finkenzeller, H., Stolzenburg, D., Iyer, S., Simon, M., Kürten, A., Shen, J.,

https://doi.org/10.5194/acp-2021-99
Preprint. Discussion started: 18 March 2021

Atmospheric Chemistry and Physics Discussions

514 Rörup, B., Rissanen, M., Schobesberger, S., Baalbaki, R., Wang, D. S., Koenig, T. K., Jokinen, T., Sarnela, N., Beck, L.,
515 Almeida, J., Amanatidis, S., Amorim, A., Ataei, F., Baccarini, A., Bertozzi, B., Bianchi, F., Brilke, S., Caudillo, L., Chen,
516 D., Chiu, R., Chu, B., Dias, A., Ding, A., Dommen, J., Duplissy, J., El-Haddad, I., Gonzalez Carracedo, L., Granzin, M.,
517 Hansel, A., Heinritzi, M., Hofbauer, V., Junninen, H., Kangasluoma, J., Kemppainen, D., Kim, C., Kong, W., Krechmer,
518 J. E., Kvashnin, A., Laitinen, T., Lamkaddam, H., Lee, C. P., Lehtipalo, K., Leiminger, M., Li, Z., Makhmutov, V.,
519 Manninen, H. E., Marie, G., Marten, R., Mathot, S., Mauldin, R. L., Mentler, B., Möhler, O., Müller, T., Nie, W., Onnela,
520 A., Petäjä, T., Pfeifer, J., Philippov, M., Ranjithkumar, A., Saiz-Lopez, A., Salma, I., Scholz, W., Schuchmann, S.,
521 Schulze, B., Steiner, G., Stozkhov, Y., Tauber, C., Tomé, A., Thakur, R. C., Väisänen, O., Vazquez-Pufleau, M., Wagner,
522 A. C., Wang, Y., Weber, S. K., Winkler, P. M., Wu, Y., Xiao, M., Yan, C., Ye, Q., Ylisirniö, A., Zauner-Wieczorek, M.,
523 Zha, Q., Zhou, P., Flagan, R. C., Curtius, J., Baltensperger, U., Kulmala, M., Kerminen, V.-M., Kurten, T., et al.: Role of
524 iodine oxoacids in atmospheric aerosol nucleation, Science, 371(6529), 589–595, doi:10.1126/science.abe0298, 2021.
525 Heinritzi, M., Dada, L., Simon, M., Stolzenburg, D., Wagner, A. C., Fischer, L., Ahonen, L. R., Amanatidis, S., Baalbaki,
526 R., Baccarini, A., Bauer, P. S., Baumgartner, B., Bianchi, F., Brilke, S., Chen, D., Chiu, R., Dias, A., Dommen, J.,
527 Duplissy, J., Finkenzeller, H., Frege, C., Fuchs, C., Garmash, O., Gordon, H., Granzin, M., El Haddad, I., He, X., Helm,
528 J., Hofbauer, V., Hoyle, C. R., Kangasluoma, J., Keber, T., Kim, C., Kürten, A., Lamkaddam, H., Laurila, T. M.,
529 Lampilahti, J., Lee, C. P., Lehtipalo, K., Leiminger, M., Mai, H., Makhmutov, V., Manninen, H. E., Marten, R., Mathot,
530 S., Mauldin, R. L., Mentler, B., Molteni, U., Müller, T., Nie, W., Nieminen, T., Onnela, A., Partoll, E., Passananti, M.,
531 Petäjä, T., Pfeifer, J., Pospisilova, V., Quéléver, L. L. J., Rissanen, M. P., Rose, C., Schobesberger, S., Scholz, W.,
532 Scholze, K., Sipilä, M., Steiner, G., Stozhkov, Y., Tauber, C., Tham, Y. J., Vazquez-Pufleau, M., Virtanen, A., Vogel, A.
533 L., Volkamer, R., Wagner, R., Wang, M., Weitz, L., Wimmer, D., Xiao, M., Yan, C., Ye, P., Zha, Q., Zhou, X., Amorim,
534 A., Baltensperger, U., Hansel, A., Kulmala, M., Tomé, A., Winkler, P. M., Worsnop, D. R., Donahue, N. M., Kirkby, J.
535 and Curtius, J.: Molecular understanding of the suppression of new-particle formation by isoprene, Atmos. Chem. Phys.,
536 20(20), 11809–11821, doi:10.5194/acp-20-11809-2020, 2020.
537 Henze, D. K., Seinfeld, J. H., Liao, W., Sandu, A. and Carmichael, G. R.: Inverse modeling of aerosol dynamics:
538 Condensational growth, J. Geophys. Res.-Atmos., 109(D14), doi:https://doi.org/10.1029/2004JD004593, 2004.
539 Kaipio, J. and Somersalo, E.: Statistical and Computational Inverse Problems, Springer-Verlag, New York., 2005.
540 Kallinger, P. and Szymanski, W. W.: Experimental determination of the steady-state charging probabilities and particle
541 size conservation in non-radioactive and radioactive bipolar aerosol chargers in the size range of 5-40 nm, J. Nanopart.
542 Res., 17(4), 171, doi:10.1007/s11051-015-2981-x, 2015.
543 Kandlikar, M. and Ramachandran, G.: Inverse methods for analysing aerosol spectrometer measurements: a critical
544 review, J. Aerosol Sci., 30(4), 413–437, doi:https://doi.org/10.1016/S0021-8502(98)00066-4, 1999.
545 Kangasluoma, J., Cai, R., Jiang, J., Deng, C., Stolzenburg, D., Ahonen, L. R., Chan, T., Fu, Y., Kim, C., Laurila, T. M.,
546 Zhou, Y., Dada, L., Sulo, J., Flagan, R. C., Kulmala, M., Petäjä, T. and Lehtipalo, K.: Overview of measurements and
547 current instrumentation for 1–10 nm aerosol particle number size distributions, J. Aerosol Sci., 105584,
548 doi:https://doi.org/10.1016/j.jaerosci.2020.105584, 2020.
549 Kirkby, J., Curtius, J., Almeida, J., Dunne, E., Duplissy, J., Ehrhart, S., Franchin, A., Gagné, S., Ickes, L., Kürten, A.,
550 Kupc, A., Metzger, A., Riccobono, F., Rondo, L., Schobesberger, S., Tsagkogeorgas, G., Wimmer, D., Amorim, A.,
551 Bianchi, F., Breitenlechner, M., David, A., Dommen, J., Downard, A., Ehn, M., Flagan, R. C., Haider, S., Hansel, A.,
552 Hauser, D., Jud, W., Junninen, H., Kreissl, F., Kvashin, A., Laaksonen, A., Lehtipalo, K., Lima, J., Lovejoy, E. R.,
553 Makhmutov, V., Mathot, S., Mikkilä, J., Minginette, P., Mogo, S., Nieminen, T., Onnela, A., Pereira, P., Petäjä, T.,

https://doi.org/10.5194/acp-2021-99
Preprint. Discussion started: 18 March 2021

Atmospheric Chemistry and Physics Discussions

554 Schnitzhofer, R., Seinfeld, J. H., Sipilä, M., Stozhkov, Y., Stratmann, F., Tomé, A., Vanhanen, J., Viisanen, Y., Vrtala,
555 A., Wagner, P. E., Walther, H., Weingartner, E., Wex, H., Winkler, P. M., Carslaw, K. S., Worsnop, D. R., Baltensperger,
556 U. and Kulmala, M.: Role of sulphuric acid, ammonia and galactic cosmic rays in atmospheric aerosol nucleation, Nature,
557 476, 429–433, doi:10.1038/nature10343, 2011.
558 Kirkby, J., Duplissy, J., Sengupta, K., Frege, C., Gordon, H., Williamson, C., Heinritzi, M., Simon, M., Yan, C., Almeida,
559 J., Tröstl, J., Nieminen, T., Ortega, I. K., Wagner, R., Adamov, A., Amorim, A., Bernhammer, A.-K., Bianchi, F.,
560 Breitenlechner, M., Brilke, S., Chen, X., Craven, J., Dias, A., Ehrhart, S., Flagan, R. C., Franchin, A., Fuchs, C., Guida,
561 R., Hakala, J., Hoyle, C. R., Jokinen, T., Junninen, H., Kangasluoma, J., Kim, J., Krapf, M., Kürten, A., Laaksonen, A.,
562 Lehtipalo, K., Makhmutov, V., Mathot, S., Molteni, U., Onnela, A., Peräkylä, O., Piel, F., Petäjä, T., Praplan, A. P.,
563 Pringle, K., Rap, A., Richards, N. A. D., Riipinen, I., Rissanen, M. P., Rondo, L., Sarnela, N., Schobesberger, S., Scott,
564 C. E., Seinfeld, J. H., Sipilä, M., Steiner, G., Stozhkov, Y., Stratmann, F., Tomé, A., Virtanen, A., Vogel, A. L., Wagner,
565 A. C., Wagner, P. E., Weingartner, E., Wimmer, D., Winkler, P. M., Ye, P., Zhang, X., Hansel, A., Dommen, J., Donahue,
566 N. M., Worsnop, D. R., Baltensperger, U., Kulmala, M., Carslaw, K. S. and Curtius, J.: Ion-induced nucleation of pure
567 biogenic particles, Nature, 533, 521–526, doi:10.1038/nature17953, 2016.
568 Kuang, C., Chen, M., Zhao, J., Smith, J., McMurry, P. H. and Wang, J.: Size and time-resolved growth rate measurements
569 of 1 to 5 nm freshly formed atmospheric nuclei, Atmos. Chem. Phys., 12(7), 3573–3589, doi:10.5194/acp-12-3573-2012,
570 2012.
571 Kulmala, M., Petäjä, T., Nieminen, T., Sipilä, M., Manninen, H. E., Lehtipalo, K., Dal Maso, M., Aalto, P. P., Junninen,
572 H., Paasonen, P., Riipinen, I., Lehtinen, K. E. J., Laaksonen, A. and Kerminen, V.-M.: Measurement of the nucleation of
573 atmospheric aerosol particles, Nat. Protoc., 7(9), 1651–1667, doi:10.1038/nprot.2012.091, 2012.
574 Kupiainen-Määttä, O.: A Monte Carlo approach for determining cluster evaporation rates from concentration
575 measurements, Atmos. Chem. Phys., 16(22), 14585–14598, doi:10.5194/acp-16-14585-2016, 2016.
576 Kürten, A., Li, C., Bianchi, F., Curtius, J., Dias, A., Donahue, N. M., Duplissy, J., Flagan, R. C., Hakala, J., Jokinen, T.,
577 Kirkby, J., Kulmala, M., Laaksonen, A., Lehtipalo, K., Makhmutov, V., Onnela, A., Rissanen, M. P., Simon, M., Sipilä,
578 M., Stozhkov, Y., Tröstl, J., Ye, P. and McMurry, P. H.: New particle formation in the sulfuric acid--dimethylamine--
579 water system: reevaluation of CLOUD chamber measurements and comparison to an aerosol nucleation and growth
580 model, Atmos. Chem. Phys., 18(2), 845–863, doi:10.5194/acp-18-845-2018, 2018.
581 Lehtinen, K. E. J. and Kulmala, M.: A model for particle formation and growth in the atmosphere with molecular
582 resolution in size, Atmos. Chem. Phys., 3(1), 251–257, doi:10.5194/acp-3-251-2003, 2003.
583 Lehtinen, K. E. J., Rannik, Ü., Petäjä, T., Kulmala, M. and Hari, P.: Nucleation rate and vapor concentration estimations
584 using a least squares aerosol dynamics method, J. Geophys. Res.-Atmos., 109(D21), doi:10.1029/2004JD004893, 2004.
585 McGuffin, D. L., Huang, Y., Flagan, R. C., Petäjä, T., Ydstie, B. E. and Adams, P. J.: Novel estimation of aerosol
586 processes with particle size distribution measurements: a case study with TOMAS algorithm, Geosci. Model Dev.
587 Discuss., 2020, 1–27, doi:10.5194/gmd-2020-281, 2020.
588 Nieminen, T., Lehtinen, K. E. J. and Kulmala, M.: Sub-10 nm particle growth by vapor condensation – effects of vapor
589 molecule size and particle thermal speed, Atmos. Chem. Phys., 10(20), 9773–9779, doi:10.5194/acp-10-9773-2010, 2010.
590 Nieminen, T., Kerminen, V.-M., Petäjä, T., Aalto, P. P., Arshinov, M., Asmi, E., Baltensperger, U., Beddows, D. C. S.,
591 Beukes, J. P., Collins, D., Ding, A., Harrison, R. M., Henzing, B., Hooda, R., Hu, M., Hõrrak, U., Kivekäs, N., Komsaare,
592 K., Krejci, R., Kristensson, A., Laakso, L., Laaksonen, A., Leaitch, W. R., Lihavainen, H., Mihalopoulos, N., Németh,
593 Z., Nie, W., O'Dowd, C., Salma, I., Sellegri, K., Svenningsson, B., Swietlicki, E., Tunved, P., Ulevicius, V., Vakkari, V.,

https://doi.org/10.5194/acp-2021-99
Preprint. Discussion started: 18 March 2021

Atmospheric Chemistry and Physics Discussions

Vana, M., Wiedensohler, A., Wu, Z., Virtanen, A. and Kulmala, M.: Global analysis of continental boundary layer new particle formation based on long-term measurements, Atmos. Chem. Phys., 18(19), 14737–14756, doi:10.5194/acp-18-14737-2018, 2018.

Ozon, M., Seppänen, A., Kaipio, J. P. and Lehtinen, K. E. J.: Retrieval of process rate parameters in the general dynamic equation for aerosols using Bayesian state estimation, Geosci. Model Dev. Discuss., 2020, 1–32, doi:10.5194/gmd-2020-236, 2020.

Pichelstorfer, L., Stolzenburg, D., Ortega, J., Karl, T., Kokkola, H., Laakso, A., Lehtinen, K. E. J., Smith, J. N., McMurry, P. H. and Winkler, P. M.: Resolving nanoparticle growth mechanisms from size- and time-dependent growth rate analysis, Atmos. Chem. Phys., 18(2), 1307–1323, doi:10.5194/acp-18-1307-2018, 2018.

Pope, C. A. and Dockery, D. W.: Health Effects of Fine Particulate Air Pollution: Lines that Connect, J. Air Waste Manag., 56(6), 709–742, doi:10.1080/10473289.2006.10464485, 2006.

Sandu, A., Liao, W., Carmichael, G. R., Henze, D. K. and Seinfeld, J. H.: Inverse Modeling of Aerosol Dynamics Using Adjoints: Theoretical and Numerical Considerations, Aerosol Sci. Tech., 39(8), 677–694, doi:10.1080/02786820500182289, 2005.

Seinfeld, J. and Pandis, S.: Atmospheric Chemistry and Physics: From Air Pollution to Climate Change, 3rd edition, 3rd editio., Wiley., 2016.

Shcherbacheva, A., Balehowsky, T., Kubečka, J., Olenius, T., Helin, T., Haario, H., Laine, M., Kurtén, T. and Vehkamäki, H.: Identification of molecular cluster evaporation rates, cluster formation enthalpies and entropies by Monte Carlo method, Atmos. Chem. Phys. Discuss., 2020, 1–58, doi:10.5194/acp-2019-1036, 2020.

Shen, J., Shu, C. and Zhang, M.: High Resolution Schemes for a Hierarchical Size-Structured Model, SIAM J. Numer. Anal., 45(1), 352–370, doi:10.1137/050638126, 2007.

Simon, M., Dada, L., Heinritzi, M., Scholz, W., Stolzenburg, D., Fischer, L., Wagner, A. C., Kürten, A., Rörup, B., He, X.-C., Almeida, J., Baalbaki, R., Baccarini, A., Bauer, P. S., Beck, L., Bergen, A., Bianchi, F., Bräkling, S., Brilke, S., Caudillo, L., Chen, D., Chu, B., Dias, A., Draper, D. C., Duplissy, J., El-Haddad, I., Finkenzeller, H., Frege, C., Gonzalez-Carracedo, L., Gordon, H., Granzin, M., Hakala, J., Hofbauer, V., Hoyle, C. R., Kim, C., Kong, W., Lamkaddam, H., Lee, C. P., Lehtipalo, K., Leiminger, M., Mai, H., Manninen, H. E., Marie, G., Marten, R., Mentler, B., Molteni, U., Nichman, L., Nie, W., Ojdanic, A., Onnela, A., Partoll, E., Petäjä, T., Pfeifer, J., Philippov, M., Quéléver, L. L. J., Ranjithkumar, A., Rissanen, M. P., Schallhart, S., Schobesberger, S., Schuchmann, S., Shen, J., Sipilä, M., Steiner, G., Stozhkov, Y., Tauber, C., Tham, Y. J., Tomé, A. R., Vazquez-Pufleau, M., Vogel, A. L., Wagner, R., Wang, M., Wang, D. S., Wang, Y., Weber, S. K., Wu, Y., Xiao, M., Yan, C., Ye, P., Ye, Q., Zauner-Wieczorek, M., Zhou, X., Baltensperger, U., Dommen, J., Flagan, R. C., Hansel, A., Kulmala, M., Volkamer, R., Winkler, P. M., Worsnop, D. R., Donahue, N. M., Kirkby, J. and Curtius, J.: Molecular understanding of new-particle formation from alpha-pinene between -50 and +25 °C, Atmos. Chem. Phys., 20(15), 9183–9207, doi:10.5194/acp-20-9183-2020, 2020.

Sipilä, M., Sarnela, N., Jokinen, T., Henschel, H., Junninen, H., Kontkanen, J., Richters, S., Kangasluoma, J., Franchin, A., Peräkylä, O., Rissanen, M. P., Ehn, M., Vehkamäki, H., Kurten, T., Berndt, T., Petäjä, T., Worsnop, D., Ceburnis, D., Kerminen, V.-M., Kulmala, M. and O'Dowd, C.: Molecular-scale evidence of aerosol particle formation via sequential addition of HIO3, Nature, 537, 532, doi:10.1038/nature19314, 2016.

Smolarkiewicz, P. K.: A fully multidimensional positive definite advection transport algorithm with small implicit diffusion, J. Comput. Phys., 54(2), 325–362, doi:https://doi.org/10.1016/0021-9991(84)90121-9, 1984.

Stolzenburg, D., Steiner, G. and Winkler, P. M.: A DMA-train for precision measurement of sub-10 nm aerosol dynamics,

634 Atmos. Meas. Tech., 10(4), 1639–1651, doi:10.5194/amt-10-1639-2017, 2017.
635 Stolzenburg, D., Fischer, L., Vogel, A. L., Heinritzi, M., Schervish, M., Simon, M., Wagner, A. C., Dada, L., Ahonen, L.
636 R., Amorim, A., Baccarini, A., Bauer, P. S., Baumgartner, B., Bergen, A., Bianchi, F., Breitenlechner, M., Brilke, S.,
637 Buenrostro Mazon, S., Chen, D., Dias, A., Draper, D. C., Duplissy, J., El Haddad, I., Finkenzeller, H., Frege, C., Fuchs,
638 C., Garmash, O., Gordon, H., He, X., Helm, J., Hofbauer, V., Hoyle, C. R., Kim, C., Kirkby, J., Kontkanen, J., Kürten,
639 A., Lampilahti, J., Lawler, M., Lehtipalo, K., Leiminger, M., Mai, H., Mathot, S., Mentler, B., Molteni, U., Nie, W.,
640 Nieminen, T., Nowak, J. B., Ojdanic, A., Onnela, A., Passananti, M., Petäjä, T., Quéléver, L. L. J., Rissanen, M. P.,
641 Sarnela, N., Schallhart, S., Tauber, C., Tomé, A., Wagner, R., Wang, M., Weitz, L., Wimmer, D., Xiao, M., Yan, C., Ye,
642 P., Zha, Q., Baltensperger, U., Curtius, J., Dommen, J., Flagan, R. C., Kulmala, M., Smith, J. N., Worsnop, D. R., Hansel,
643 A., Donahue, N. M. and Winkler, P. M.: Rapid growth of organic aerosol nanoparticles over a wide tropospheric
644 temperature range, P. Nat. Acad. Sci. USA, 115(37), 9122–9127, doi:10.1073/pnas.1807604115, 2018.
645 Stolzenburg, D., Simon, M., Ranjithkumar, A., Kürten, A., Lehtipalo, K., Gordon, H., Ehrhart, S., Finkenzeller, H.,
646 Pichelstorfer, L., Nieminen, T., He, X.-C., Brilke, S., Xiao, M., Amorim, A., Baalbaki, R., Baccarini, A., Beck, L.,
647 Bräkling, S., Caudillo Murillo, L., Chen, D., Chu, B., Dada, L., Dias, A., Dommen, J., Duplissy, J., El Haddad, I., Fischer,
648 L., Gonzalez Carracedo, L., Heinritzi, M., Kim, C., Koenig, T. K., Kong, W., Lamkaddam, H., Lee, C. P., Leiminger, M.,
649 Li, Z., Makhmutov, V., Manninen, H. E., Marie, G., Marten, R., Müller, T., Nie, W., Partoll, E., Petäjä, T., Pfeifer, J.,
650 Philippov, M., Rissanen, M. P., Rörup, B., Schobesberger, S., Schuchmann, S., Shen, J., Sipilä, M., Steiner, G., Stozhkov,
651 Y., Tauber, C., Tham, Y. J., Tomé, A., Vazquez-Pufleau, M., Wagner, A. C., Wang, M., Wang, Y., Weber, S. K., Wimmer,
652 D., Wlasits, P. J., Wu, Y., Ye, Q., Zauner-Wieczorek, M., Baltensperger, U., Carslaw, K. S., Curtius, J., Donahue, N. M.,
653 Flagan, R. C., Hansel, A., Kulmala, M., Lelieveld, J., Volkamer, R., Kirkby, J. and Winkler, P. M.: Enhanced growth rate
654 of atmospheric particles from sulfuric acid, Atmos. Chem. Phys., 20(12), 7359–7372, doi:10.5194/acp-20-7359-2020,
655 2020.
656 Stolzenburg, M. R. and McMurry, P. H.: Equations Governing Single and Tandem DMA Configurations and a New
657 Lognormal Approximation to the Transfer Function, Aerosol Sci. Tech., 42, 421–432, doi:10.1080/02786820802157823,
658 2008.
659 Tauber, C., Schmoll, D., Gruenwald, J., Brilke, S., Wlasits, P. J., Winkler, P. M. and Wimmer, D.: Characterization of a
660 Non-Thermal Plasma Source for the Use as a Mass Spec Calibration Tool and Non-Radioactive Aerosol Charger, Atmos.
661 Meas. Tech., 13(11), 5993–6006, doi:10.5194/amt-13-5993-2020, 2020.
662 Tröstl, J., Chuang, W. K., Gordon, H., Heinritzi, M., Yan, C., Molteni, U., Ahlm, L., Frege, C., Bianchi, F., Wagner, R.,
663 Simon, M., Lehtipalo, K., Williamson, C., Craven, J. S., Duplissy, J., Adamov, A., Almeida, J., Bernhammer, A.-K.,
664 Breitenlechner, M., Brilke, S., Dias, A., Ehrhart, S., Flagan, R. C., Franchin, A., Fuchs, C., Guida, R., Gysel, M., Hansel,
665 A., Hoyle, C. R., Jokinen, T., Junninen, H., Kangasluoma, J., Keskinen, H., Kim, J., Krapf, M., Kürten, A., Laaksonen,
666 A., Lawler, M., Leiminger, M., Mathot, S., Möhler, O., Nieminen, T., Onnela, A., Petäjä, T., Piel, F. M., Miettinen, P.,
667 Rissanen, M. P., Rondo, L., Sarnela, N., Schobesberger, S., Sengupta, K., Sipilä, M., Smith, J. N., Steiner, G., Tomè, A.,
668 Virtanen, A., Wagner, A. C., Weingartner, E., Wimmer, D., Winkler, P. M., Ye, P., Carslaw, K. S., Curtius, J., Dommen,
669 J., Kirkby, J., Kulmala, M., Riipinen, I., Worsnop, D. R., Donahue, N. M. and Baltensperger, U.: The role of low-volatility
670 organic compounds in initial particle growth in the atmosphere, Nature, 533, 527–531, doi:10.1038/nature18271, 2016.
671 Twomey, S.: Pollution and the planetary albedo, Atmos. Environ., 8(12), 1251–1256, doi:https://doi.org/10.1016/0004-
672 6981(74)90004-3, 1974.
673 Verheggen, B. and Mozurkewich, M.: An inverse modeling procedure to determine particle growth and nucleation rates

https://doi.org/10.5194/acp-2021-99
Preprint. Discussion started: 18 March 2021

Atmospheric Chemistry and Physics Discussions

674 from measured aerosol size distributions, Atmos. Chem. Phys., 6(10), 2927–2942, doi:10.5194/acp-6-2927-2006, 2006.
675 Viskari, T., Asmi, E., Kolmonen, P., Vuollekoski, H., Petäjä, T. and Järvinen, H.: Estimation of aerosol particle number
676 distributions with Kalman Filtering – Part 1: Theory, general aspects and statistical validity, Atmos. Chem. Phys., 12(24),
677 11767–11779, doi:10.5194/acp-12-11767-2012, 2012.
678 Wiedensohler, A.: An approximation of the bipolar charge distribution for particles in the submicron size range, J. Aerosol
679 Sci., 19(3), 387–389, doi:10.1016/0021-8502(88)90278-9, 1988.
680 Wlasits, P. J., Stolzenburg, D., Tauber, C., Brilke, S., Schmitt, S. H., Winkler, P. M. and Wimmer, D.: Counting on
681 chemistry: laboratory evaluation of seed-material-dependent detection efficiencies of ultrafine condensation particle
682 counters, Atmos. Meas. Tech., 13(7), 3787–3798, doi:10.5194/amt-13-3787-2020, 2020.
683 Wolfenbarger, J. K. and Seinfeld, J. H.: Inversion of aerosol size distribution data, J. Aerosol Sci., 21(2), 227–247,
684 doi:https://doi.org/10.1016/0021-8502(90)90007-K, 1990.
685